

Global Neutrino Constraints on the Minimal $U(1)_{L_\mu - L_\tau}$ Model

Masahiro Ibe^{a,b}, Satoshi Shirai^b and Keiichi Watanabe^a

^a *ICRR, The University of Tokyo, Kashiwa, Chiba 277-8582, Japan*

^b *Kavli Institute for the Physics and Mathematics of the Universe (WPI),
The University of Tokyo Institutes for Advanced Study,
The University of Tokyo, Kashiwa 277-8583, Japan*

Abstract

We examine the minimal $U(1)_{L_\mu - L_\tau}$ gauge model in light of the latest neutrino data, including neutrino oscillations, cosmological observations, direct mass measurements, and neutrinoless double-beta decay. Using the most conservative oscillation data, we find that normal ordering is excluded at approximately the 90% confidence level (CL). Incorporating cosmological constraints from Cosmic Microwave Background (CMB) observations strengthens this exclusion to about 95% CL, while further including Baryon Acoustic Oscillation (BAO) data increases it to nearly 99% CL. The inverted ordering is even more strongly disfavored. Our analysis is performed within a frequentist framework, minimizing sensitivity to prior assumptions inherent in Bayesian approaches. These results impose strong constraints on the viability of the minimal $U(1)_{L_\mu - L_\tau}$ gauge model.

1 Introduction

The $U(1)_{L_\mu-L_\tau}$ gauge symmetry [1–7] has long been an intriguing subject of study within the particle phenomenology community as one of the simplest extensions of the Standard Model (SM) that remains consistent with experimental constraints. In particular, the minimal $U(1)_{L_\mu-L_\tau}$ model, where the symmetry is spontaneously broken by the vacuum expectation value of a single $U(1)_{L_\mu-L_\tau}$ charged scalar field, realizes the two-zero minor neutrino mass structure [8, 9]. This leads to high predictive power for neutrino oscillation phenomena, which has therefore gathered significant attention in the context of neutrino physics.

Furthermore, the model has potential implications for the anomalous magnetic moment of the muon ($g - 2$) when the gauge boson mass of $U(1)_{L_\mu-L_\tau}$ lies in the sub-GeV region. At present, it remains uncertain whether a discrepancy exists between the experimental measurements [10–12] of the muon’s anomalous magnetic moment and the SM predictions [13].¹ However, if such a discrepancy is confirmed, the $U(1)_{L_\mu-L_\tau}$ symmetry is widely regarded as a well-motivated extension that could account for this anomaly. Various experimental searches for this model are actively underway (see e.g., Refs. [15–22]).

On the other hand, as pointed out in Refs. [23–25], the high predictive power of the minimal $U(1)_{L_\mu-L_\tau}$ model strongly constrains it through the results of neutrino oscillation experiments and cosmological observations, particularly constraints on the sum of neutrino masses. Consequently, analyses based on the latest data suggest that this model is increasingly entering a region in conflict with observational results.

In this paper, we investigate the extent to which the minimal $U(1)_{L_\mu-L_\tau}$ model is statistically disfavored based on the latest data from neutrino oscillation experiments, direct mass measurements, neutrinoless double-beta decay, Cosmic Microwave Background (CMB) observations, and Baryon Acoustic Oscillation (BAO) observations. Our analysis shows that, under the assumption of the Λ CDM model, the minimal $U(1)_{L_\mu-L_\tau}$ model is excluded at the 99% confidence level (CL). This result suggests that reviving the minimal $U(1)_{L_\mu-L_\tau}$ model would require significant modifications beyond the Λ CDM framework. It is important to note that our results apply specifically to the minimal $U(1)_{L_\mu-L_\tau}$ model and do not exclude the possibility of more complex extensions.

The organization of this paper is as follows. In Sec. 2, we summarize a minimal gauged $U(1)_{L_\mu-L_\tau}$ model. In Sec. 3, we analyze this model from the perspective of frequentist statistics. The final section is devoted to our conclusions.

Table 1: Charge assignments of leptons and ϕ under $U(1)_{L_\mu - L_\tau}$ gauge symmetry. All other SM fields not listed in this table are neutral under this symmetry.

Field		$U(1)_{L_\mu - L_\tau}$	
Leptons	L_e	\bar{e}_e	\bar{N}_e
	L_μ	\bar{e}_τ	\bar{N}_τ
	L_τ	\bar{e}_μ	\bar{N}_μ
Scalar		ϕ	+1

2 Minimal $U(1)_{L_\mu - L_\tau}$ Model

We summarize the minimal gauged $U(1)_{L_\mu - L_\tau}$ model in Refs. [23–25]. The model extends the SM by introducing three right-handed neutrinos $\bar{N}_{e,\mu,\tau}$ and a complex scalar ϕ .² This model has a new $U(1)$ symmetry under which leptons and ϕ have $U(1)$ charges shown in Tab. 1. All other particles not listed in the table do not have this $U(1)_{L_\mu - L_\tau}$ charge.

Note that in a renormalizable model where there is only one complex scalar field that spontaneously breaks $U(1)_{L_\mu - L_\tau}$ symmetry, the (type-I) seesaw mechanism [27–31] is the minimal setup to reproduce the neutrino oscillation experiments. With the gauge charges given in Tab. 1, the interaction terms responsible for neutrino mass and mixing are given by,

$$\mathcal{L} = - \sum_{i=e,\mu,\tau} \kappa_i L_i \bar{N}_i H - \frac{1}{2} M_{ee} \bar{N}_e \bar{N}_e - M_{\mu\tau} \bar{N}_\mu \bar{N}_\tau - \kappa_{e\mu} \bar{N}_e \bar{N}_\mu \phi - \kappa_{e\tau} \bar{N}_e \bar{N}_\tau \phi^\dagger + \text{h.c.} \quad (2.1)$$

Here, H denotes the SM Higgs doublet. Due to the $U(1)_{L_\mu - L_\tau}$ gauge symmetry, the Yukawa interactions of the charged leptons are diagonal, $\kappa_{e,\mu,\tau}$. Moreover, by exploiting the phase freedom of the singlet charged leptons, these Yukawa couplings can be made real and positive without loss of generality. Similarly, the Yukawa interactions κ_i between the right-handed neutrinos and the lepton doublets are also diagonal, and can be rendered real and positive by utilizing the phase freedom of the lepton doublets. Additionally, the mass terms M_{ee} and $M_{\mu\tau}$ can be made real and positive through the phase rotations of the right-handed neutrinos. However, it is not possible to simultaneously render both $\kappa_{e\mu}$ and $\kappa_{e\tau}$ real-valued using phase transformations. Consequently, the minimal $U(1)_{L_\mu - L_\tau}$ model inherently contains a single physical parameter responsible for CP violation.

After the H and ϕ acquire their vacuum expectation values (VEVs), $\langle H \rangle = (0, v_{\text{EW}})^T$ and

¹The theoretical prediction of the muon anomalous magnetic moment ($g - 2$) remains somewhat unclear at present. Currently, discrepancies between data-driven approaches and lattice simulations have been reported (see Ref. [14] and references therein).

²In this paper, all the fermions are denoted by the Weyl fermion with the notation used in Ref. [26].

$\langle \phi \rangle = v_\phi$, respectively, the following mass terms arise:

$$\mathcal{L} = -m_{D,ij} L_i \bar{N}_i - \frac{1}{2} M_{R,ij} \bar{N}_i \bar{N}_j + \text{h.c.} , \quad (2.2)$$

where m_D and M_R are expressed as

$$m_D = v_{\text{EW}} \begin{pmatrix} \kappa_e & 0 & 0 \\ 0 & \kappa_\mu & 0 \\ 0 & 0 & \kappa_\tau \end{pmatrix} , \quad M_R = \begin{pmatrix} M_{ee} & \kappa_{e\mu} v_\phi & \kappa_{e\tau} v_\phi \\ \kappa_{e\mu} v_\phi & 0 & M_{\mu\tau} \\ \kappa_{e\tau} v_\phi & M_{\mu\tau} & 0 \end{pmatrix} . \quad (2.3)$$

By integrating out the right-handed neutrinos, the mass matrix of light neutrino are given by the seesaw mechanism [27–31],

$$m_\nu = -m_D M_R^{-1} m_D^T . \quad (2.4)$$

This matrix is a complex symmetric matrix and can be diagonalized using the Takagi decomposition with a single unitary matrix,

$$m_\nu = U^* \hat{m}_\nu U^\dagger , \quad \hat{m}_\nu = \text{diag}(m_1, m_2, m_3) , \quad (2.5)$$

where $m_{1,2,3}$ are taken real positive. The neutrino mass parameters are ordered

$$m_1 < m_2 < m_3 , \quad (2.6)$$

for the normal ordering (NO) case, and

$$m_3 < m_1 < m_2 , \quad (2.7)$$

for the inverted ordering (IO) case. As the charged lepton sector has been diagonalized, the unitary matrix U above is identified as the PMNS matrix with Majorana phases, and its parametrization is given by the following expression,

$$U = \begin{pmatrix} U_{e1} & U_{e2} & U_{e3} \\ U_{\mu 1} & U_{\mu 2} & U_{\mu 3} \\ U_{\tau 1} & U_{\tau 2} & U_{\tau 3} \end{pmatrix} = \begin{pmatrix} c_{12}c_{13} & s_{12}c_{13} & s_{13}e^{-i\delta_{\text{CP}}} \\ -s_{12}c_{23} - c_{12}s_{13}s_{23}e^{i\delta_{\text{CP}}} & c_{12}c_{23} - s_{12}s_{13}s_{23}e^{i\delta_{\text{CP}}} & c_{13}s_{23} \\ s_{12}s_{23} - c_{12}s_{13}c_{23}e^{i\delta_{\text{CP}}} & -c_{12}s_{23} - s_{12}s_{13}c_{23}e^{i\delta_{\text{CP}}} & c_{13}c_{23} \end{pmatrix} \begin{pmatrix} e^{i\eta_1} & 0 & 0 \\ 0 & e^{i\eta_2} & 0 \\ 0 & 0 & 1 \end{pmatrix} , \quad (2.8)$$

where $c_{ij} := \cos \theta_{ij}$ and $s_{ij} := \sin \theta_{ij}$. Phases δ_{CP} and $\eta_{1,2}$ are the Dirac phase and the Majorana phases.

Due to the two-zero texture of M_R and Eq. (2.4), m_ν^{-1} has two zeros in the (μ, μ) and (τ, τ) entries. Those two-zero minor structures lead to the following constraints [23, 32, 33],

$$r_{21} := \frac{m_2}{m_1} = \left(1 - \frac{\csc \theta_{12}}{\sin \theta_{12} + e^{i\delta_{\text{CP}}} \cos \theta_{12} \sin \theta_{13} \tan 2\theta_{23}} \right) \times e^{-2i(\eta_1 - \eta_2)} , \quad (2.9)$$

$$r_{31} := \frac{m_3}{m_1} = \frac{-\cos^2 \theta_{13} [2 \cos^2 \theta_{12} \cos 2\theta_{23} - \sin 2\theta_{12} \sin 2\theta_{23} \sin \theta_{13} e^{i\delta_{\text{CP}}}]}{\sin \theta_{13} [2 \cos 2\theta_{12} \cos 2\theta_{23} \sin \theta_{13} - \sin 2\theta_{12} \sin 2\theta_{23} (e^{-i\delta_{\text{CP}}} + \sin^2 \theta_{13} e^{i\delta_{\text{CP}}})]} \times e^{-i(2\delta_{\text{CP}} + 2\eta_1)} . \quad (2.10)$$

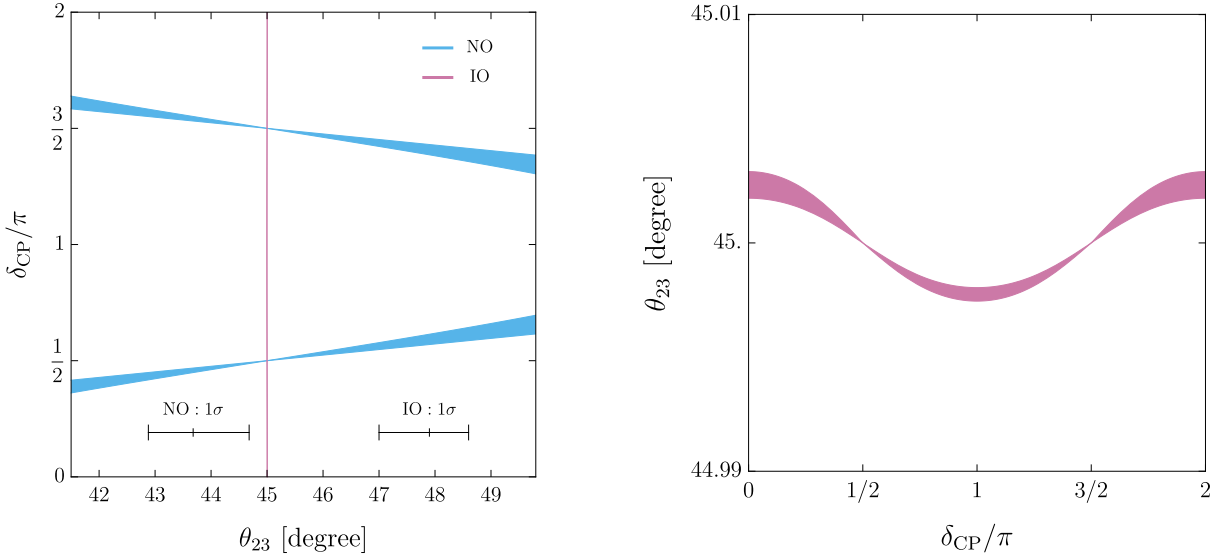


Figure 1: The correlation between δ_{CP} and the mixing parameters in the minimal $U(1)_{L_\mu - L_\tau}$ model. The blue lines show δ_{CP} as a function of θ_{23} for the NO case. In the left figure, the purple vertical line indicates the predicted value $\theta_{23} \simeq \pi/4$ for the IO case, which is closed up in the right panel. Mixing parameters and $R_{\text{NO,IO}}$ are varied within their 3σ ranges according to NuFIT 6.0 (IC24 with SK-atm), where the 1σ ranges of θ_{23} are indicated by bars.

The Majorana phases $\eta_{1,2}$ are fixed to ensure positive-definite neutrino masses.

To see the correlation between parameters, let us consider the ratio between the solar and atmospheric mass-squared differences,

$$R_{\text{NO}} := \frac{\Delta m_{21}^2}{\Delta m_{31}^2} = \frac{r_{21}^2 - 1}{r_{31}^2 - 1} , \quad (2.11)$$

for the NO case and

$$R_{\text{IO}} := \frac{\Delta m_{12}^2}{\Delta m_{32}^2} = \frac{1 - r_{21}^2}{r_{31}^2 - r_{21}^2} , \quad (2.12)$$

for the IO case. Then, by taking the observed values of $R_{\text{NO,IO}}$ extracted from NuFIT 6.0 [34], we show the correlation between θ_{23} and δ_{CP} in Fig. 1. Other parameters and the value of R are varied within their 3σ ranges according to NuFIT 6.0 (IC24 with SK-atm), where the 1σ ranges of θ_{23} are indicated by bars.

For the NO case, the correlation between the mixing angles and δ_{CP} can be understood as follows. From Eq. (2.10), we find that r_{31} is at most $\mathcal{O}(1)$. Thus, the observed value $R_{\text{NO}} = \mathcal{O}(10^{-2})$ is realized only when $r_{21} \simeq 1$, which leads to

$$\cos \delta_{\text{CP}} \simeq \cot 2\theta_{12} \cot 2\theta_{23} \csc \theta_{13} . \quad (2.13)$$

Using the best-fit values of the mixing angles from NuFIT 6.0, we obtain $\cos \delta_{\text{CP}} \simeq 0.17$, corresponding to δ_{CP} values around $\pi/2$ and $3\pi/2$ for the NO case.

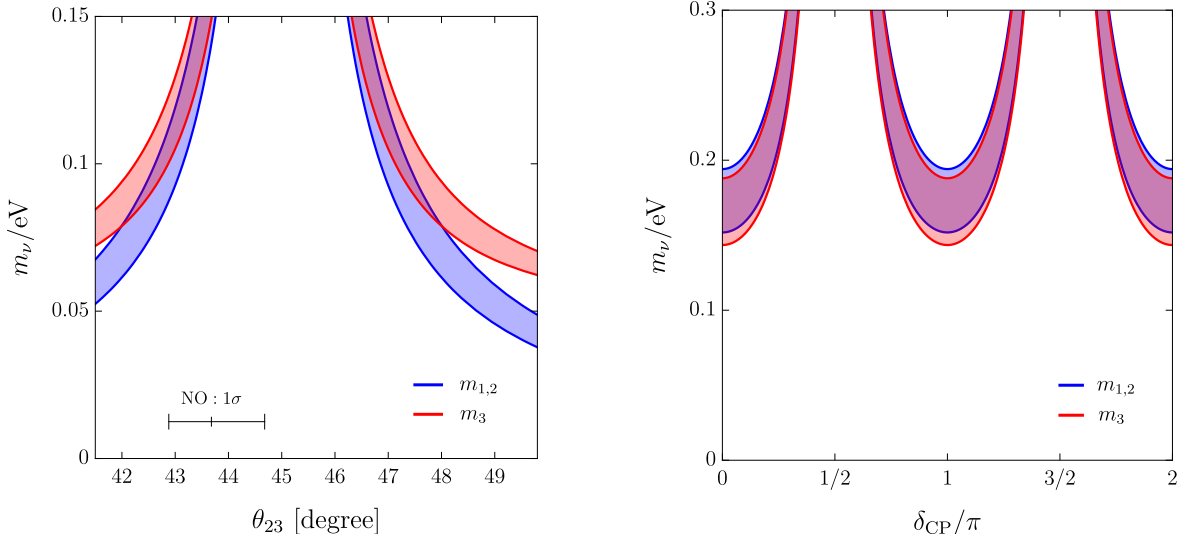


Figure 2: The neutrino mass spectrum as a function of θ_{23} for the NO case (left) and δ_{CP} for the IO case (right), varying the mixing parameters within their 3σ ranges based on NuFIT 6.0 (IC24 with SK-atm). For the IO case, θ_{23} is in the vicinity of $\pi/4$.

For the IO case, on the other hand, the correlation emerges along $\theta_{23} \simeq \pi/4$, where $r_{21} \simeq 1$. Expanding s_{23} around $\theta_{23} \simeq \pi/4$ as $s_{23} \simeq 1/\sqrt{2} + \epsilon$ ($|\epsilon| \ll 1$), we find

$$r_{21} \simeq 1 + \frac{4\sqrt{2} \cos \delta_{\text{CP}}}{\sin \theta_{13} \sin 2\theta_{12}} \epsilon + \mathcal{O}(\epsilon^2) . \quad (2.14)$$

Thus, the observed value $R_{\text{IO}} = \mathcal{O}(10^{-2})$ can be achieved with a small ϵ .

For both the NO and IO cases, we find that $r_{21} \simeq 1$, implying

$$m_1^2, m_2^2 \gg \Delta m_{21}^2 , \quad (2.15)$$

which indicates that m_1 and m_2 are nearly degenerate. Figure 2 presents the neutrino mass spectrum as a function of θ_{23} for the NO case and δ_{CP} for the IO case, with the oscillation parameters varied within their 3σ ranges based on NuFIT 6.0 (IC24 with SK-atm). For the NO case, the spectrum exhibits mild degeneracy between m_3 and $m_{1,2}$, whereas in the IO case, the masses are fully degenerate, particularly near $\theta_{23} \simeq \pi/4$. This strong degeneracy results in a relatively large total neutrino mass in the minimal $U(1)_{L_\mu - L_\tau}$ model. As discussed in the next section, cosmological observations impose stringent constraints on the total neutrino mass, placing significant restrictions on the model's viability.

Before closing this section, we briefly comment on the radiative corrections to the two-zero minor structure of the neutrino mass matrix. At the leading order, this structure remains invariant under renormalization group running below the seesaw scale. However, at the one-loop level, finite threshold corrections from the $U(1)_{L_\mu - L_\tau}$ gauge symmetry breaking sector induce right-handed neutrino mass terms, $M_{\mu\mu}$ and $M_{\tau\tau}$, proportional to $\kappa_{e\mu}^2 \langle \phi \rangle^2$ and $\kappa_{e\tau}^2 \langle \phi^\dagger \rangle^2$, respectively. As a consequence, the

two-zero minor structure is explicitly broken at one loop. In this study, we assume that the couplings between the $U(1)_{L_\mu-L_\tau}$ -breaking field and the right-handed neutrinos are sufficiently small, allowing us to neglect these corrections.

3 Analysis and Result

Neutrino physics is characterized by nine parameters: the three neutrino masses, three mixing angles, and three CP phases. In the $U(1)_{L_\mu-L_\tau}$ model, imposing the two-zero minor condition leads to the constraints in Eqs. (2.9) and (2.10), which reduces the number of free parameters by four, leaving a total of five. To constrain the $U(1)_{L_\mu-L_\tau}$ model, one can apply a likelihood ratio test based on Wilks' theorem, comparing the full neutrino model with its $U(1)_{L_\mu-L_\tau}$ -restricted counterpart to derive parameter constraints.

Tables 2 and 3 summarize the results. The first row indicates the type of observational data used in the analysis, along with $\Delta\chi^2$ and the exclusion confidence level (CL). Here, $\Delta\chi^2$ is defined as the difference between the χ^2 minima of the restricted model (minimal $U(1)_{L_\mu-L_\tau}$ model) and the full model. From the second row onward, the table specifies the data included in each analysis, where “-” denotes that the corresponding dataset was not used.

Following the convention of NuFIT, we present two sets of results for the IceCube experiment and Super-Kamiokande atmospheric neutrino data: “IC19 w/o SK-atm” and “IC24 with SK-atm.” A dagger (\dagger) next to the exclusion confidence level indicates that the value is determined solely by neutrino oscillation data. The details of the analysis will be discussed later.

The tables show that, using the most conservative oscillation data, NO is excluded at approximately the 90% CL. Incorporating cosmological constraints from the Planck 2020 PR4 analysis strengthens this exclusion to about 95% CL, while further including BAO data increases it to nearly 99% CL. For the IO case, even with the most conservative neutrino oscillation data, the model is excluded at the 92% CL. With the addition of cosmological constraints, even the most conservative limits from Planck 2020 PR4 exclude the model at a significance of 4.4σ .

3.1 Neutrino oscillation

First, we conduct a likelihood analysis of the minimal $U(1)_{L_\mu-L_\tau}$ model based on neutrino oscillation experiments using data from NuFIT 6.0 [34]. NuFIT provides two analyses: “IC19 w/o SK-atm,” which utilizes IceCube/DeepCore (IC) 3-year data (2012–2015) [35, 36], and “IC24 with SK-atm,” which incorporates the χ^2 map of IC 9.3-year data (2012–2021) [37] along with the χ^2 map of 484.2 kiloton-year Super-Kamiokande atmospheric data [38].

Neutrino oscillations are parameterized by six key variables:

$$\Delta m_{21}^2, \quad \Delta m_{3\ell}^2, \quad (3.1)$$

$$\sin^2 \theta_{12}, \quad \sin^2 \theta_{13}, \quad \sin^2 \theta_{23}, \quad \delta_{\text{CP}}. \quad (3.2)$$

Table 2: Constraints on the NO case using NuFIT 6.0 oscillation data. The results are presented separately for analyses **IC19 w/o SK-atm** and **IC24 with SK-atm**. Each row includes additional constraints from direct neutrino mass measurements (m_β), neutrinoless double beta decay ($0\nu\beta\beta$) with different nuclear matrix elements ($M^{0\nu}$), and cosmological observations (Planck, Planck + DESI). The confidence levels (CL) or statistical significance (σ) are reported for each case.

Oscillation	m_β	$0\nu\beta\beta$	Cosmology	$\Delta\chi^2(\text{NO})$	Confidence Level
IC19 w/o SK-atm (NuFIT 6.0)					
NuFIT 6.0	-	-	-	2.7	90% CL
NuFIT 6.0	KATRIN	-	-	2.9	90% CL [†]
NuFIT 6.0	-	$M^{0\nu} = 1.11$	-	5.1	90% CL [†]
NuFIT 6.0	-	$M^{0\nu} = 2.39$	-	7.6	90% CL [†]
NuFIT 6.0	-	$M^{0\nu} = 4.77$	-	10	97% CL
NuFIT 6.0	-	-	Planck	6.6	96% CL
NuFIT 6.0	-	-	Planck + DESI	13	3.2σ
IC24 with SK-atm (NuFIT 6.0)					
NuFIT 6.0	-	-	-	4.3	96% CL
NuFIT 6.0	KATRIN	-	-	4.4	96% CL [†]
NuFIT 6.0	-	$M^{0\nu} = 1.11$	-	3.8	90% CL [†]
NuFIT 6.0	-	$M^{0\nu} = 2.39$	-	7.4	90% CL [†]
NuFIT 6.0	-	$M^{0\nu} = 4.77$	-	15	2.8σ
NuFIT 6.0	-	-	Planck	5.8	94% CL
NuFIT 6.0	-	-	Planck + DESI	16	3.6σ

Although NuFIT 6.0 provides comprehensive χ^2 data for these parameters, it does not include the full six-dimensional χ^2 function. Instead, it offers χ^2 tables marginalized over subsets of three, two, or one variable(s), denoted as χ_{3D} , χ_{2D} , and χ_{1D} , respectively, where all other parameters are optimized to minimize χ^2 . These marginalized χ^2 values satisfy the relation

$$\chi_{\text{full}}^2(\Delta m_{21}^2, \Delta m_{3\ell}^2, \sin^2 \theta_{12}, \sin^2 \theta_{13}, \sin^2 \theta_{23}, \delta_{\text{CP}}) \geq \chi_{3D}^2(x, y, z) \geq \chi_{2D}^2(x, y) \geq \chi_{1D}^2(x) , \quad (3.3)$$

where x , y , and z represent the oscillation parameters. It is important to note that χ_{full}^2 is not sensitive to the absolute neutrino mass nor two Majorana phases.

To ensure a conservative treatment of model constraints, we define the effective χ^2 , χ_{eff}^2 , used in our analysis as:

$$\chi_{\text{eff}}^2(\Delta m_{21}^2, \Delta m_{3\ell}^2, \sin^2 \theta_{12}, \sin^2 \theta_{13}, \sin^2 \theta_{23}, \delta_{\text{CP}}) = \max [\chi_{3D}^2(\Delta m_{3\ell}^2, \sin^2 \theta_{23}, \delta_{\text{CP}}), \chi_{2D}^2(x, y), \chi_{1D}^2(x)] . \quad (3.4)$$

This definition ensures that χ_{eff}^2 is always equal to or smaller than the full χ^2 , χ_{full}^2 , providing a conservative basis for evaluating model constraints. In the subsequent analysis of neutrino oscillations, we perform a maximum likelihood estimation (i.e., the least χ^2) using χ_{eff}^2 , which is projected onto the total neutrino mass:

$$m_{\text{tot}} = m_1 + m_2 + m_3 . \quad (3.5)$$

Table 3: Same as Tab. 2, but for the IO case.

Oscillation	m_β	$0\nu\beta\beta$	Cosmology	$\Delta\chi^2(\text{IO})$	Confidence Level
IC19 w/o SK-atm (NuFIT 6.0)					
NuFIT 6.0	-	-	-	5.8	98% CL
NuFIT 6.0	KATRIN	-	-	9.1	2.6σ
NuFIT 6.0	-	$M^{0\nu} = 1.11$	-	20	3.5σ
NuFIT 6.0	-	$M^{0\nu} = 2.39$	-	65	7.3σ
NuFIT 6.0	-	-	Planck	24	4.6σ
NuFIT 6.0	-	-	Planck + DESI	68	8.1σ
IC24 with SK-atm (NuFIT 6.0)					
NuFIT 6.0	-	-	-	3.1	92% CL
NuFIT 6.0	KATRIN	-	-	7.1	97% CL
NuFIT 6.0	-	$M^{0\nu} = 1.11$	-	18	3.2σ
NuFIT 6.0	-	$M^{0\nu} = 2.39$	-	63	7.2σ
NuFIT 6.0	-	-	Planck	23	4.4σ
NuFIT 6.0	-	-	Planck + DESI	68	8.0σ

In Fig. 3, we plot, for each m_{tot} , the difference in χ^2_{eff} between two cases: one where the neutrino oscillation parameters are varied to minimize χ^2_{eff} under the constraints of the minimal $U(1)_{L_\mu - L_\tau}$ model, and another where all six parameters are freely varied to minimize χ^2_{eff} . The latter is denoted as χ^2_{min} . For the IC24 with SK-atm analysis, we find that $\chi^2_{\text{min}} = 0$ for the NO case and $\chi^2_{\text{min}} = 6.1$ for the IO case. In contrast, for the IC19 w/o SK-atm analysis, $\chi^2_{\text{min}} = 0.6$ for the NO case and $\chi^2_{\text{min}} = 0$ for the IO case (see Ref. [34]).

It is important to note that the constraints in Eqs. (2.9) and (2.10) reduce the number of parameters by two, one of which corresponds to the absolute neutrino mass and is thus irrelevant for χ^2_{eff} . Consequently, due to Wilks' theorem, the minimum value of the difference $\chi^2_{\text{eff}} - \chi^2_{\text{min}}$ follows a χ^2 distribution with one degree of freedom.³ The minimum values of $\chi^2_{\text{eff}} - \chi^2_{\text{min}}$ are summarized in Tabs. 2 and 3. For the IO case, this minimum value is reached in the limit $m_{\text{tot}} \rightarrow \infty$, where $\theta_{23} \rightarrow \pi/4$.

3.2 Direct neutrino mass measurement

The KATRIN experiment directly probes the absolute neutrino mass scale by analyzing the kinematics of tritium β -decay [39]. By examining the endpoint region of the electron energy spectrum, KATRIN constrains the effective electron neutrino mass, which is defined as

$$m_\beta^2 = \sum_i |U_{ei}|^2 m_i^2 . \quad (3.6)$$

³Strictly speaking, this statement holds for χ^2_{full} . However, since χ^2_{eff} provides a conservative estimate of χ^2_{full} , we assume that it also holds for χ^2_{eff} in the following discussion.

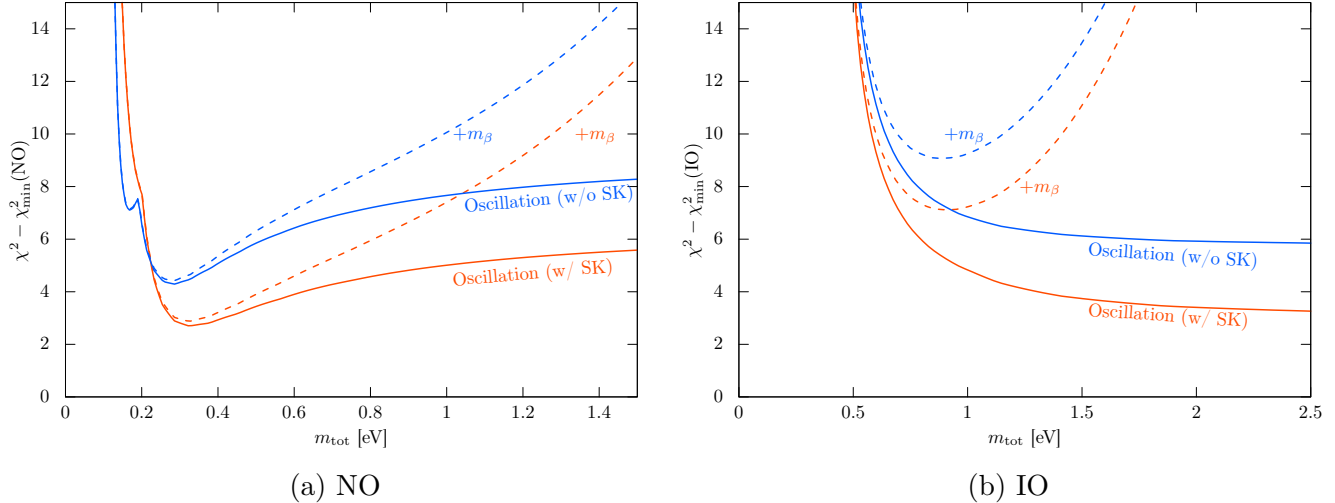


Figure 3: The difference in χ_{eff}^2 between two cases: one where the neutrino oscillation parameters are varied to minimize χ_{eff}^2 under the constraints of the minimal $U(1)_{L_\mu - L_\tau}$ model, and another where all six parameters are freely varied to minimize χ_{eff}^2 . The latter is denoted as χ_{min}^2 . Panel (a) corresponds to the NO case, while panel (b) corresponds to the IO case. The red (blue) curves are based on χ^2 data from NuFIT 6.0 “IC24 without SK-atm” (“IC19 w/o SK-atm”). The dashed lines represent cases that, in addition to oscillation data, data from the direct neutrino mass measurement by KATRIN is included.

Through a detailed spectral shape analysis near the endpoint, KATRIN places an upper bound on m_β , finding no significant deviation from the standard massless neutrino hypothesis [40],

$$m_\beta < 0.45 \text{ eV (90\% CL)} . \quad (3.7)$$

We extract the χ^2 values for m_β^2 from Ref. [40] and fit them with a quadratic function. Figure 4 shows $\Delta\chi^2$ as a function of m_β , with the blue line representing the fitted result. The dashed lines in Fig. 3 illustrate $\Delta\chi^2$ when KATRIN data is incorporated into the neutrino oscillation analysis.

Note that the estimation of m_β requires knowledge of the full PMNS matrix and all three neutrino masses. In the minimal $U(1)_{L_\mu - L_\tau}$ model, the constraints in Eqs. (2.9) and (2.10) impose two relations among m_1 , m_2 , and m_3 . As a result, when applying Wilks’ theorem, the χ^2 test must be performed with two degrees of freedom.

One important point should be emphasized here. For instance, when comparing the $\Delta\chi^2$ values between the analysis using only oscillation data in Tab. 2 and the analysis incorporating direct neutrino mass measurement results, the latter yields slightly larger values. However, as discussed above, the latter requires a χ^2 analysis with two degrees of freedom. Consequently, the constraints obtained from this combined analysis are weaker than those derived solely from neutrino oscillation data. This indicates that incorporating additional information into the analysis does not necessarily strengthen the constraints.

This can be understood as follows. Wilks’ theorem assumes that the likelihood ratio test statistic

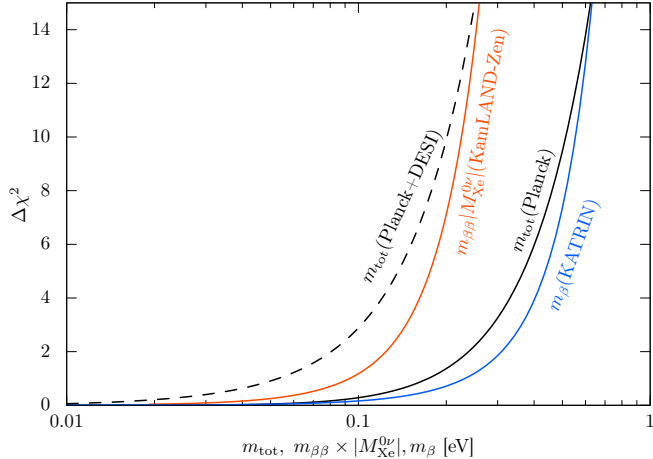


Figure 4: The $\Delta\chi^2$ values for the various neutrino mass parameters. The blue solid line represents $\Delta\chi^2$ from the direct mass measurement by KATRIN as a function of m_β in Eq. (3.6). The red solid line corresponds to $\Delta\chi^2$ from neutrinoless double-beta decay measured by KamLAND-ZEN as a function of $m_{\beta\beta} \times |M_{\text{Xe}}^{0\nu}|$ in Eq. (3.8). The black solid (dashed) lines indicate $\Delta\chi^2$ from the cosmological observation of the total neutrino mass by Planck (Planck+DESI).

follows a χ^2 distribution, which in turn requires the Fisher information matrix to be well-conditioned. In the present case, some eigenvalues of the Fisher information matrix can be nearly zero, indicating that certain parameter directions are weakly constrained. As a result, the likelihood function deviates from a quadratic form near its maximum, leading to a breakdown of the χ^2 approximation underlying Wilks' theorem. In such cases, relying solely on neutrino oscillation data provides a more conservative bound, as indicated by \dagger in Tab. 2.

3.3 Neutrinoless double-beta decay

In the present model, neutrinos have Majorana masses, which leads to lepton number violating processes. The rates of these processes increase proportionally to the square of the neutrino mass. Currently, no lepton number violating processes have been observed experimentally, with the strongest constraints coming from neutrinoless double-beta ($0\nu\beta\beta$) decay in nuclei.

The decay half-life of a nucleus via the ($0\nu\beta\beta$) decay, $T_{1/2}^{0\nu}$, is given by

$$\frac{1}{T_{1/2}^{0\nu}} = G^{0\nu} |M_{\text{Xe}}^{0\nu}|^2 \frac{m_{\beta\beta}^2}{m_e^2} , \quad (3.8)$$

where $G^{0\nu}$ is the phase-space factor, $M_{\text{Xe}}^{0\nu}$ is the nuclear matrix element of ^{136}Xe , $m_{\beta\beta}$ is the effective Majorana neutrino mass, and m_e is the electron mass (see Ref. [14] for a review). The effective Majorana neutrino mass is defined as

$$m_{\beta\beta} = \left| \sum_i U_{ei}^2 m_i \right| . \quad (3.9)$$

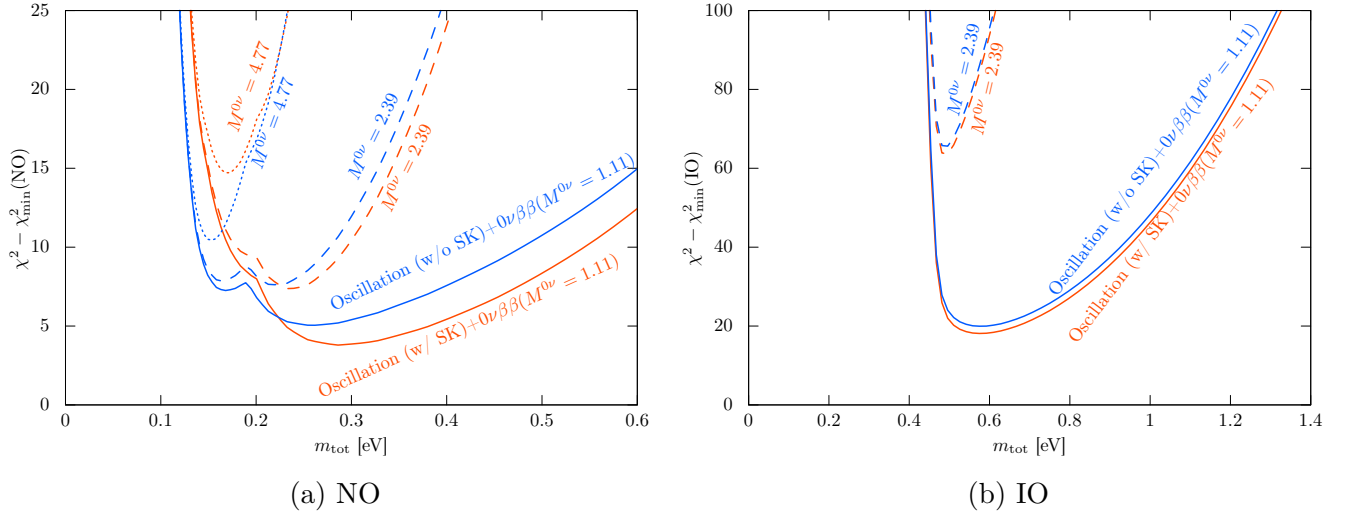


Figure 5: The values of $\Delta\chi^2$ incorporating both neutrino oscillation data and neutrinoless double-beta decay data from KamLAND-ZEN.

KamLAND-ZEN experiment searches for $(0\nu\beta\beta)$ decay using ^{136}Xe , and so far, no signals have been detected, which places $T_{1/2}^{0\nu} > 3.8 \times 10^{26}$ yr at 90% CL [41]. In this paper, we obtain the χ^2 for $m_{\beta\beta}$ using data from KamLAND-ZEN. We perform a fit for the background and signal in the observed spectrum within the energy range $2.35 \text{ MeV} < E < 2.70 \text{ MeV}$. Considering the uncertainty in the nuclear matrix element, the χ^2 is evaluated for the product $m_{\beta\beta} \times |M_{\text{Xe}}^{0\nu}|$. In Fig. 4, we show the $\Delta\chi^2$ in red line. Following the KamLAND-ZEN analysis, we analyze the range

$$1.11 \leq |M_{\text{Xe}}^{0\nu}| \leq 4.77 , \quad (3.10)$$

for the nuclear matrix element uncertainty (see also e.g., Ref. [42] for review). Fig. 5 presents $\Delta\chi^2$ as a function of m_{tot} , incorporating information from neutrino oscillations and $m_{\beta\beta}$. For parameters other than m_{tot} , the values that minimize $\Delta\chi^2$ are used, while multiple possibilities for the matrix elements are considered.

The estimation of $m_{\beta\beta}$ requires all neutrino parameters, including the Majorana phases. In the case of the minimal $U(1)_{L_\mu-L_\tau}$ model, the constraints given in Eqs. (2.9) and (2.10) reduce the number of free parameters by four in terms of real degrees of freedom. Accordingly, when applying Wilks' theorem, a χ^2 test should be performed with four degrees of freedom.

3.4 Cosmology

Current upper limits on m_{tot} from cosmological observation range from approximately 0.1 eV to 0.5 eV at 95% CL, depending on the likelihood profile, datasets, and the adopted cosmological model (see Ref. [14] for a review). In the following analysis, we assume the ΛCDM model and use the likelihood profile provided in Ref. [43]. In particular, for the CMB constraints, we use the likelihood profile obtained from `HILLiPoP23-PR4+Lensing-PR3` [44–47], where the known lensing

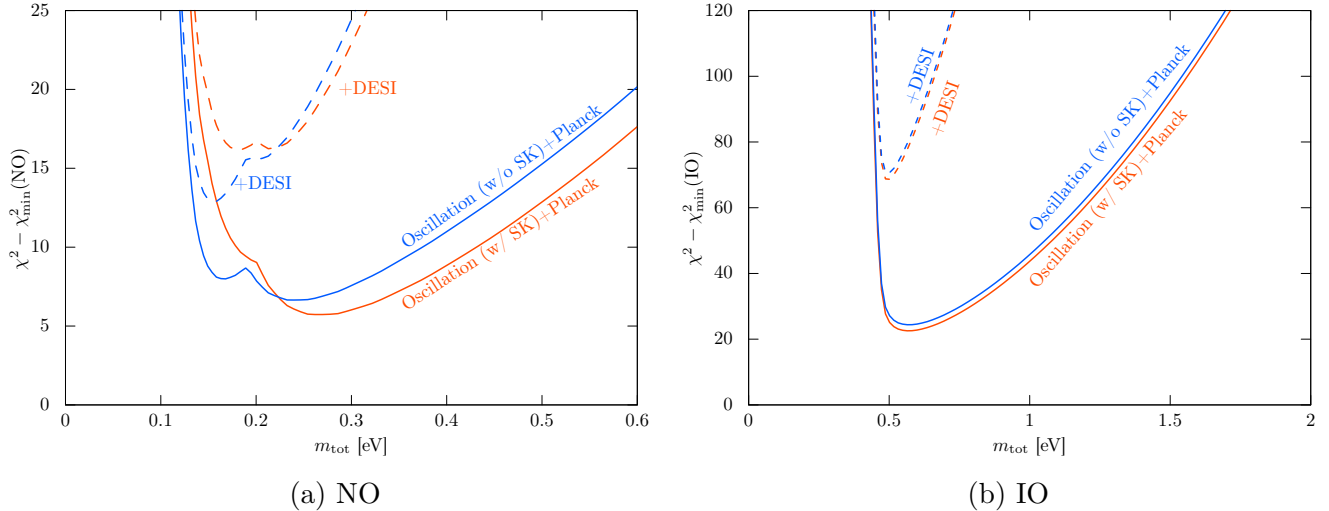


Figure 6: The $\Delta\chi^2$ values as a function of m_{tot} . The blue (red) solid line represents $\Delta\chi^2$ obtained using the NuFIT 6.0 data without (with) SK consideration. The cosmological data used are from Planck and DESI.

anomaly present in the Planck 2018 Plik likelihood [48] is significantly reduced. For the BAO constraints, we adopt the DESI-Y1-no07 dataset, which excludes the $z = 0.7$ bin identified as a 2.6σ outlier in the DESI-Y1 results [49, 50]. According to the analysis in Ref. [43], the combination of HilliPoP23-PR4+Lensing-PR3 and DESI-Y1-no07 provides the maximally conservative constraint from the combined CMB and BAO observations within the Λ CDM model. In Fig. 4, we show those profile likelihoods. Figure 6 shows $\Delta\chi^2$ as a function of m_{tot} , incorporating information from neutrino oscillations and cosmology. Note that as in the case of the χ^2 analysis with the direct neutrino mass measurement, the χ^2 test must be performed with two degrees of freedom.

4 Conclusion

In this work, we examined the minimal $U(1)_{L_\mu - L_\tau}$ gauge model in light of the latest neutrino data, incorporating results from neutrino oscillation experiments, cosmological observations, direct neutrino mass measurements, and searches for neutrinoless double-beta decay. Our analysis was conducted within a frequentist framework to ensure robustness against prior-dependent uncertainties.

Using the most conservative neutrino oscillation data, we found that normal ordering (NO) is excluded at approximately the 90% confidence level (CL). Incorporating cosmological constraints from the Planck 2020 PR4 analysis strengthens this exclusion to about 95% CL, while further including BAO data increases it to nearly 99% CL. For the inverted ordering (IO) case, the constraints are even more severe, with oscillation data alone excluding it at the 92% CL, and additional cosmological constraints leading to a statistical significance of 4.4σ .

The primary reason for this exclusion is the model's predictive structure, which leads to a nearly

degenerate neutrino mass spectrum. This results in a large total neutrino mass, which is strongly constrained by cosmological data. Additionally, neutrinoless double-beta decay and direct neutrino mass measurements impose further restrictions on the parameter space.

Our results indicate that the minimal $U(1)_{L_\mu - L_\tau}$ gauge model is increasingly disfavored under the assumption of the Λ CDM framework. Reviving this model would require significant modifications, such as introducing additional fields that alters the two-zero minor structure of the neutrino mass matrix or relax the stringent cosmological constraints.

Future advancements in neutrino physics, particularly improved measurements of the absolute neutrino mass scale and cosmological constraints, will further test the viability of this model. If stronger constraints on the total neutrino mass emerge, the minimal $U(1)_{L_\mu - L_\tau}$ scenario may be entirely ruled out, necessitating a reconsideration of its role in particle physics.

In this analysis, we have neglected finite threshold corrections from the $U(1)_{L_\mu - L_\tau}$ gauge symmetry breaking sector. However, if the relevant couplings are sufficiently strong, these corrections could disrupt the two-zero minor structure of the neutrino mass matrix. A more detailed investigation of these effects would be worthwhile.

Acknowledgements

This work is supported by Grant-in-Aid for Scientific Research from the Ministry of Education, Culture, Sports, Science, and Technology (MEXT), Japan, 21H04471, 22K03615, 24K23938 (M.I.), 20H01895 and 20H05860 (S.S.) and by World Premier International Research Center Initiative (WPI), MEXT, Japan. This work is supported by JST SPRING, Grant Number JPMJSP2108 and ANRI fellowship (K.W.).

References

- [1] R. Foot, Mod. Phys. Lett. A **6**, 527 (1991).
- [2] X.-G. He, G. C. Joshi, H. Lew, and R. R. Volkas, Phys. Rev. D **44**, 2118 (1991).
- [3] R. Foot, X. G. He, H. Lew, and R. R. Volkas, Phys. Rev. D **50**, 4571 (1994), arXiv:hep-ph/9401250 .
- [4] S. N. Gninenko and N. V. Krasnikov, Phys. Lett. B **513**, 119 (2001), arXiv:hep-ph/0102222 .
- [5] S. Baek, N. G. Deshpande, X. G. He, and P. Ko, Phys. Rev. D **64**, 055006 (2001), arXiv:hep-ph/0104141 .
- [6] B. Murakami, Phys. Rev. D **65**, 055003 (2002), arXiv:hep-ph/0110095 .
- [7] E. Ma, D. P. Roy, and S. Roy, Phys. Lett. B **525**, 101 (2002), arXiv:hep-ph/0110146 .

[8] L. Lavoura, Phys. Lett. B **609**, 317 (2005), arXiv:hep-ph/0411232 .

[9] E. I. Lashin and N. Chamoun, Phys. Rev. D **78**, 073002 (2008), arXiv:0708.2423 [hep-ph] .

[10] G. W. Bennett *et al.* (Muon g-2), Phys. Rev. D **73**, 072003 (2006), arXiv:hep-ex/0602035 .

[11] B. Abi *et al.* (Muon g-2), Phys. Rev. Lett. **126**, 141801 (2021), arXiv:2104.03281 [hep-ex] .

[12] T. Albahri *et al.* (Muon g-2), Phys. Rev. D **103**, 072002 (2021), arXiv:2104.03247 [hep-ex] .

[13] T. Aoyama *et al.*, Phys. Rept. **887**, 1 (2020), arXiv:2006.04822 [hep-ph] .

[14] S. Navas *et al.* (Particle Data Group), Phys. Rev. D **110**, 030001 (2024).

[15] R. Harnik, J. Kopp, and P. A. N. Machado, JCAP **07**, 026 (2012), arXiv:1202.6073 [hep-ph] .

[16] S. Bilmis, I. Turan, T. M. Aliev, M. Deniz, L. Singh, and H. T. Wong, Phys. Rev. D **92**, 033009 (2015), arXiv:1502.07763 [hep-ph] .

[17] J. P. Lees *et al.* (BaBar), Phys. Rev. D **94**, 011102 (2016), arXiv:1606.03501 [hep-ex] .

[18] M. Ibe, W. Nakano, and M. Suzuki, Phys. Rev. D **95**, 055022 (2017), arXiv:1611.08460 [hep-ph] .

[19] R. Capdevilla, D. Curtin, Y. Kahn, and G. Krnjaic, JHEP **04**, 129 (2022), arXiv:2112.08377 [hep-ph] .

[20] I. Adachi *et al.* (Belle-II), Phys. Rev. Lett. **131**, 121802 (2023), arXiv:2306.12294 [hep-ex] .

[21] I. Adachi *et al.* (Belle-II), Phys. Rev. D **109**, 112015 (2024), arXiv:2403.02841 [hep-ex] .

[22] Y. M. Andreev *et al.* (NA64), Phys. Rev. D **110**, 112015 (2024), arXiv:2409.10128 [hep-ex] .

[23] K. Asai, K. Hamaguchi, and N. Nagata, Eur. Phys. J. C **77**, 763 (2017), arXiv:1705.00419 [hep-ph] .

[24] K. Asai, K. Hamaguchi, N. Nagata, S.-Y. Tseng, and K. Tsumura, Phys. Rev. D **99**, 055029 (2019), arXiv:1811.07571 [hep-ph] .

[25] K. Asai, K. Hamaguchi, N. Nagata, and S.-Y. Tseng, JCAP **11**, 013 (2020), arXiv:2005.01039 [hep-ph] .

[26] H. K. Dreiner, H. E. Haber, and S. P. Martin, Phys. Rept. **494**, 1 (2010), arXiv:0812.1594 [hep-ph] .

[27] P. Minkowski, Phys. Lett. B **67**, 421 (1977).

[28] T. Yanagida, Conf. Proc. C **7902131**, 95 (1979); T. Yanagida, Phys. Rev. D **20**, 2986 (1979).

[29] M. Gell-Mann, P. Ramond, and R. Slansky, Conf. Proc. C **790927**, 315 (1979), arXiv:1306.4669 [hep-th] .

[30] S. L. Glashow, NATO Sci. Ser. B **61**, 687 (1980).

[31] R. N. Mohapatra and G. Senjanovic, Phys. Rev. Lett. **44**, 912 (1980).

[32] S. Verma, Nucl. Phys. B **854**, 340 (2012), arXiv:1109.4228 [hep-ph] .

[33] J. Liao, D. Marfatia, and K. Whisnant, JHEP **09**, 013 (2014), arXiv:1311.2639 [hep-ph] .

[34] I. Esteban, M. C. Gonzalez-Garcia, M. Maltoni, I. Martinez-Soler, J. a. P. Pinheiro, and T. Schwetz, JHEP **12**, 216 (2024), NuFit 6.0 at <http://www.nu-fit.org/>, arXiv:2410.05380 [hep-ph] .

[35] M. G. Aartsen *et al.* (IceCube), Phys. Rev. D **99**, 032007 (2019), arXiv:1901.05366 [hep-ex] .

[36] M. G. Aartsen *et al.* (IceCube), Eur. Phys. J. C **80**, 9 (2020), arXiv:1902.07771 [hep-ex] .

[37] R. Abbasi *et al.* (IceCube), (2024), arXiv:2405.02163 [hep-ex] .

[38] T. Wester *et al.* (Super-Kamiokande), Phys. Rev. D **109**, 072014 (2024), arXiv:2311.05105 [hep-ex] .

[39] J. Angrik *et al.* (KATRIN), (2005).

[40] M. Aker *et al.* (Katrín), (2024), arXiv:2406.13516 [nucl-ex] .

[41] S. Abe *et al.* (KamLAND-Zen), (2024), arXiv:2406.11438 [hep-ex] .

[42] J. J. Gómez-Cadenas, J. Martín-Albo, J. Menéndez, M. Mezzetto, F. Monrabal, and M. Sorel, Riv. Nuovo Cim. **46**, 619 (2023).

[43] D. Naredo-Tuero, M. Escudero, E. Fernández-Martínez, X. Marcano, and V. Poulin, Phys. Rev. D **110**, 123537 (2024), arXiv:2407.13831 [astro-ph.CO] .

[44] M. Tristram *et al.*, Astron. Astrophys. **682**, A37 (2024), arXiv:2309.10034 [astro-ph.CO] .

[45] M. Tristram *et al.*, Phys. Rev. D **105**, 083524 (2022), arXiv:2112.07961 [astro-ph.CO] .

[46] M. Tristram *et al.*, Astron. Astrophys. **647**, A128 (2021), arXiv:2010.01139 [astro-ph.CO] .

[47] N. Aghanim *et al.* (Planck), Astron. Astrophys. **641**, A1 (2020), arXiv:1807.06205 [astro-ph.CO] .

- [48] N. Aghanim *et al.* (Planck), Astron. Astrophys. **641**, A6 (2020), [Erratum: Astron. Astrophys. 652, C4 (2021)], arXiv:1807.06209 [astro-ph.CO] .
- [49] A. G. Adame *et al.* (DESI), (2024), arXiv:2404.03000 [astro-ph.CO] .
- [50] A. G. Adame *et al.* (DESI), JCAP **01**, 124 (2025), arXiv:2404.03001 [astro-ph.CO] .